

Low-Energy Thermal Photons from Meson-Meson Bremsstrahlung

W. Liu and R. Rapp¹

¹*Cyclotron Institute and Physics Department, Texas A&M University, College Station, Texas 77843-3366*
(Dated: May 20, 2018)

Within an effective hadronic model including electromagnetic interactions via a $U_{em}(1)$ gauge, we reinvestigate photon Bremsstrahlung from a hot hadronic gas as expected to be formed in relativistic heavy-ion collisions at SPS energies. We calculate photon emission from the reactions $\pi\pi \rightarrow \pi\pi\gamma$ and $\pi K \rightarrow \pi K\gamma$ by an explicit (numerical) evaluation of the multi-dimensional phase space integral. This, in particular, allows to avoid the commonly employed soft photon approximation (SPA), as well as to incorporate final-state thermal enhancement factors. Both improvements are shown to result in an appreciable increase of the photon production rate over previous hadronic calculations. Upon convolution over a thermal fireball we find an improvement in the description of recent low transverse-momentum WA98 data at SPS. The influence of both Landau-Pomeranchuk-Migdal and in-medium effects on “ σ ” and ρ -meson exchanges are briefly discussed.

PACS numbers: relativistic heavy-ion collisions, photon spectra, Bremsstrahlung

I. INTRODUCTION

A hot deconfined state of matter called quark-gluon plasma (QGP) is predicted to have existed during the first few microseconds after the big bang. Ultrarelativistic heavy-ion collisions (URHICs) provide the only way to recreate such matter for a short moment in the laboratory. Electromagnetic radiation is expected to be a unique probe in the study of URHICs, as the (real and virtual) photons, once produced, decouple from the strongly interacting hot matter. Since photons are emitted throughout the entire evolution of the fireball, including QGP and hadronic phases, their spectra carry valuable information on the various environments of their creation.

Studies of photon emission from hot and dense matter in heavy-ion collisions have a long history both theoretically and experimentally, cf., e.g., Refs. [1, 2, 3, 4, 5] for recent reviews. While scattering in deconfined matter is expected to mostly manifest itself in the photon spectra at transverse momenta above $q_t \simeq 2$ GeV, the hadronic stages are likely to dominate the emission at low q_t [6, 7, 8, 9, 10, 11, 12, 13]. The latter regime has recently received renewed interest due to measurements of the WA98 collaboration in central $Pb-Pb$ collisions at the CERN Super Proton Synchrotron (SPS) [14, 15]. Using Hanbury Brown-Twiss (HBT) interferometry methods, a direct photon signal could be extracted in the range of $q_t = 0.1 - 0.3$ GeV [15]. These data exhibit a large excess over theoretical predictions [11, 13] that have previously shown agreement with data for the same system (and by the same experiment) [14] at higher momenta, $q_t \geq 1.5$ GeV (where the more conventional subtraction method enabled the extraction of a direct photon excess). In subsequent work [13, 16, 17], the role of photon Bremsstrahlung from elastic π - π interactions, which was not included in the previous calculations, has been re-assessed. It was found that the Bremsstrahlung contribution notably increases the spectral yield at low q_t by up to 50% over the baseline predictions, but still significantly falls short of the WA98 data [15].

The main objective of the present work is to revisit thermal Bremsstrahlung from elastic meson-meson interactions. Based on an effective hadronic Lagrangian, with electromagnetic interactions implemented via $U_{em}(1)$ gauging, we improve the accuracy of earlier analyses by going beyond the commonly employed soft photon approximation (SPA) [18], and extend the calculations to the strangeness sector (π - K scattering). In the context of soft dileptons, corrections to the SPA have been found to be sizable and positive [19]. Our approach furthermore enables the explicit inclusion of thermal final-state enhancement factors, as well as meson-chemical potentials which arise in the hadronic evolution of URHICs after hadrochemical freezeout. As an indication of the uncertainties in applications to heavy-ion data, we briefly discuss other meson-meson Bremsstrahlung sources [12], as well as schematic estimates of medium effects in the scalar π - π channel (dropping σ mass) and of the Landau-Pomeranchuk-Migdal (LPM) effect [20, 21]. The π - π and π - K Bremsstrahlung rates are then combined with earlier hadronic emission calculations [11] and convoluted over a thermal fireball model for central $Pb-Pb$ collisions at SPS in order to put the improvements into context with the recent low-momentum WA98 data [15].

Our article is organized as follows. In Sec. II we introduce the chiral effective Lagrangian that will be used to evaluate amplitudes for elastic π - π and π - K interactions, with parameters fixed to reproduce the corresponding vacuum scattering data in Born approximation. In Sec. III, we discuss our treatment of the basic kinetic theory expression to calculate Bremsstrahlung from π - π and π - K scattering in a thermal bath. We first construct the pertinent scattering amplitudes by gauging the hadronic Lagrangian (Sec. III A), with special care to maintain electromagnetic gauge invariance by implementing appropriate contact interactions (4-point vertices). We then give a detailed account of

the various features that govern the emission rate (Sec. III B), with emphasis on the improvements over previous evaluations. In Sec. IV we illustrate further uncertainties when applying low-energy rates to heavy-ion collisions in terms of schematic estimates of the LPM effect (Sec. IV A) and medium modifications of the exchanged ρ and σ mesons (Sec. IV B). In Sec. V, the soft photon production rate is applied to calculate photon spectra in central Pb - Pb collisions at SPS, which are supplemented with earlier calculations and compared to experimental data from WA98. In Sec. VI, we estimate the coherent photon emission from initial scattering of protons within both projectile and target nuclei. Sec. VII contains a summary and discussion.

II. ELASTIC MESON-MESON SCATTERING

In this work we focus on photon Bremsstrahlung induced by elastic interactions of the lightest constituents in a hadronic gas, i.e., pion-pion (π - π) and pion-kaon (π - K) scattering (the latter will turn out to produce a factor of 4-5 less low-energy photons than the former; other contributions will be briefly discussed at the end of Sec. III B). We first recall the underlying model [9, 22] that will allow us reproduce vacuum scattering data and thus form the basis to evaluate the pertinent Bremsstrahlung processes, $\pi^a \pi^b \rightarrow \pi^1 \pi^2 \gamma$ and $\pi^a K^b \rightarrow \pi^1 K^2 \gamma$. Starting point is a chiral Lagrangian for the pseudoscalar fields (π and K) [23] where the low-lying vector mesons, ρ and K^* , are introduced via a covariant derivative leading to

$$\begin{aligned} \mathcal{L} = & g_{\sigma\pi\pi} \sigma \partial_\mu \vec{\pi} \cdot \partial^\mu \vec{\pi} + g_{\rho\pi\pi} \vec{\rho}^\mu \cdot (\vec{\pi} \times \partial_\mu \vec{\pi}) + i g_{\rho K K} (\vec{K} \vec{\tau} \partial_\mu K - \partial_\mu \vec{K} \vec{\tau} K) \cdot \vec{\rho}^\mu \\ & - i g_{\pi K K^*} (\vec{K} \vec{\tau} K^{*\mu} \cdot \partial_\mu \vec{\pi} - \partial_\mu \vec{K} \vec{\tau} K^{*\mu} \cdot \vec{\pi}) + \text{h.c.} \end{aligned} \quad (1)$$

Since we will restrict ourselves to the Born approximation, an additional (chirally invariant) σ - π - π interaction vertex with a low-mass “ σ ”-meson [24] has been added to adequately account for S -wave π - π scattering near threshold. The corresponding Feynman diagrams, comprising s , t and u channel exchanges, are depicted in Fig. 1. The pertinent

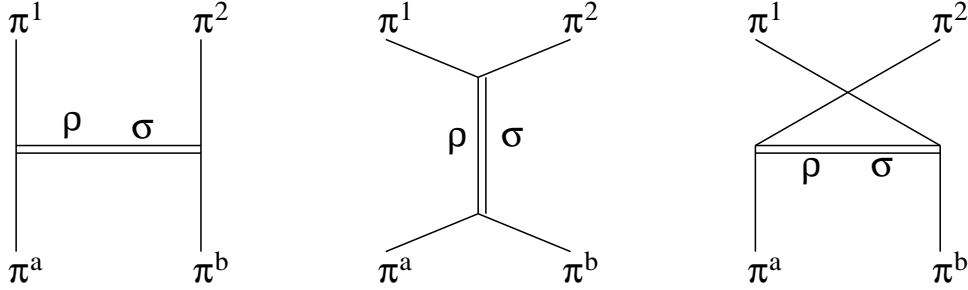


FIG. 1: Diagrams for $\pi^a \pi^b \rightarrow \pi^1 \pi^2$ scattering.

amplitudes for elastic $\pi^+ \pi^-$ scattering in t - and s -channel are given by

$$\begin{aligned} \mathcal{M}_t(p_a, p_b, p_1, p_2) &= \frac{-4g_{\sigma\pi\pi}^2 F^2(t)(p_a \cdot p_1)(p_b \cdot p_2)}{t - m_\sigma^2 + im_\sigma \Gamma_\sigma} + \frac{-g_{\rho\pi\pi}^2 F^2(t)(p_a \cdot p_b + p_a \cdot p_2 + p_b \cdot p_1 + p_1 \cdot p_2)}{t - m_\rho^2 + im_\rho \Gamma_\rho}, \\ \mathcal{M}_s(p_a, p_b, p_1, p_2) &= \frac{-4g_{\sigma\pi\pi}^2 (p_a \cdot p_b)(p_1 \cdot p_2)}{s - m_\sigma^2 + im_\sigma \Gamma_\sigma} + \frac{g_{\rho\pi\pi}^2 (p_a \cdot p_1 - p_a \cdot p_2 + p_b \cdot p_2 - p_b \cdot p_1)}{s - m_\rho^2 + im_\rho \Gamma_\rho}. \end{aligned} \quad (2)$$

To account for the finite size of the hadronic vertices, we introduce a momentum-transfer damping monopole formfactor, $F(q^2)$, for the t and u channels [9, 22],

$$F(q^2) = \frac{m_\alpha^2 - m_\pi^2}{m_\alpha^2 - q^2}, \quad (3)$$

where m_α is the mass of the exchanged meson and q the four-momentum transfer (for simplicity, we neglect formfactors for s -channel polegraphs). The differential cross section for $\pi^+ \pi^- \rightarrow \pi^+ \pi^-$ then follows as

$$\frac{d\sigma}{dt} = \frac{|\mathcal{M}_t + \mathcal{M}_s|^2}{64\pi s p_{in}^2}, \quad (4)$$

with $p_{in} = \sqrt{(s - 4m_\pi^2)}/2$ the initial pion three-momentum in the center-of-mass (cm) frame. Fixing the parameters in the non-strange sector as in Refs. [9, 22], $m_\sigma = 0.525$ GeV, $\Gamma_\sigma = 0.1$ GeV, $g_{\sigma\pi\pi} m_\sigma = 1.85$, $m_\rho = 0.775$ GeV,

$\Gamma_\rho = 0.155$ GeV and $g_{\rho\pi\pi} = 6.15$, provides a fair fit to the total $\pi\pi$ cross section [25] up to a cm energy of ~ 1 GeV, cf. left panel of Fig. 2. We neglect the contribution from the $f_2(1270)$ tensor meson as its thermal density is a factor of ~ 25 smaller than ρ -density. In the right panel, we display the decomposition into σ - and ρ -meson exchanges which

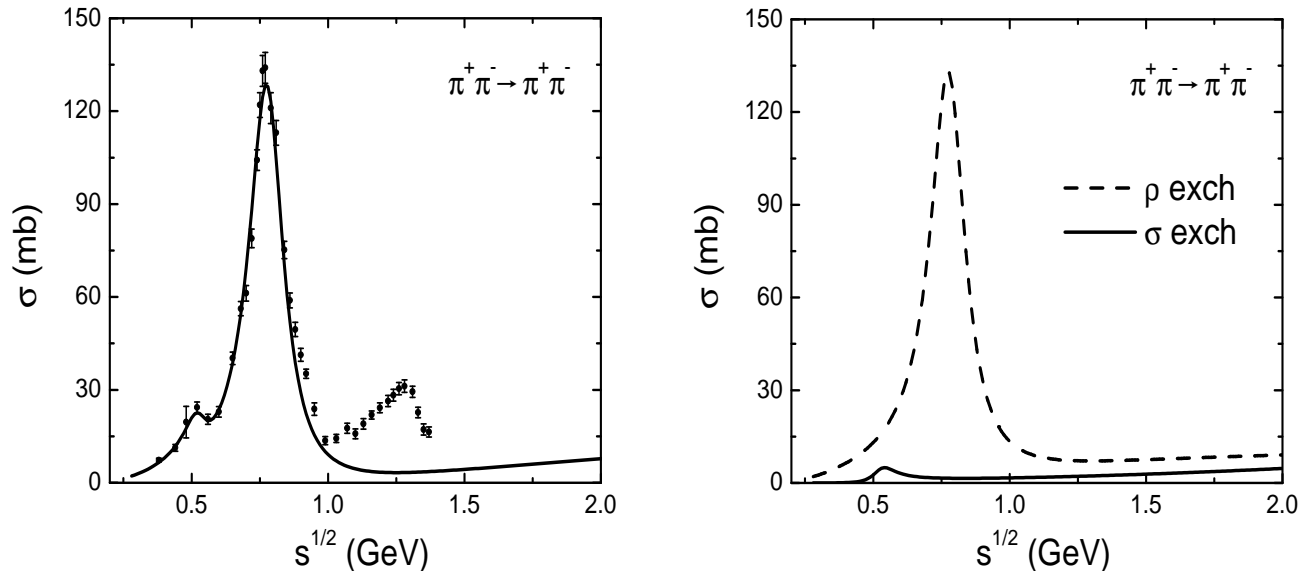


FIG. 2: Left panel: data on the elastic $\pi^+\pi^- \rightarrow \pi^+\pi^-$ cross section [25] compared to a fit using a meson-exchange model in Born approximation. Right panel: decomposition of the cross section into contributions from σ - and ρ -exchange.

identifies the s -channel ρ -polegraph as the prevalent contribution to elastic $\pi^+\pi^-$ scattering, while the one from σ -exchange is small.

Next, we turn to π - K scattering, Bremsstrahlung off which could be significant due to both the kaon's relatively large abundance in the hadronic fireball and its resonance cross section via the K^* resonance. The relevant Feynman diagrams follow from Fig. 1 by replacing one of each in- and outgoing pion by a kaon, and the ρ by K^* (no σ -exchange), resulting in sixteen processes with charged particles in the initial and/or final state. The corresponding amplitudes for elastic $\pi^-K^+ \rightarrow \pi^-K^+$ scattering are given by

$$\begin{aligned} \mathcal{M}_t(p_a, p_b, p_1, p_2) &= \frac{-g_{\rho\pi\pi}g_{\rho KK}F^2(t)(p_a \cdot p_b + p_a \cdot p_2 + p_b \cdot p_1 + p_1 \cdot p_2)}{t - m_\rho^2 + im_\rho\Gamma_\rho} \\ \mathcal{M}_s(p_a, p_b, p_1, p_2) &= \frac{2g_{\pi KK^*}^2}{s - m_{K^*}^2 + im_{K^*}\Gamma_{K^*}} \left[(p_a \cdot p_1 - p_a \cdot p_2 + p_b \cdot p_2 - p_b \cdot p_1) \right. \\ &\quad \left. - \frac{(m_\pi^2 - m_K^2)(p_a \cdot p_1 - p_a \cdot p_2 + p_b \cdot p_1 - p_b \cdot p_2)}{m_{K^*}^2} \right]. \end{aligned} \quad (5)$$

As before, the hadronic t - and u -channel vertices are augmented by a formfactor,

$$F(q^2) = \frac{\Lambda^2 - m_\alpha^2}{\Lambda_\alpha^2 - q^2}, \quad (6)$$

which is of the same form as above but with a slightly different parameter dependence which facilitates a better fit to the free scattering data. Applying Eq. (4) and fixing $\Lambda = 1.5$ GeV, $\Gamma_{K^*} = 0.051$ GeV, $g_{\rho KK} = g_{\pi KK^*} = 3.55$, and $m_{K^*} = 0.89$ GeV, the empirical cross section for elastic $\pi^-K^+ \rightarrow \pi^-K^+$ scattering [26] is reasonably well described, cf. Fig. 3.

III. THERMAL PHOTON EMISSION RATE

In kinetic theory, and to leading order in the e.m. coupling constant $\alpha_{em} = 1/137$, the thermal emission rate (per unit four-volume) of photons of energy $q_0 = q$ for a Bremsstrahlung process of type $a + b \rightarrow 1 + 2 + \gamma$ can be cast into

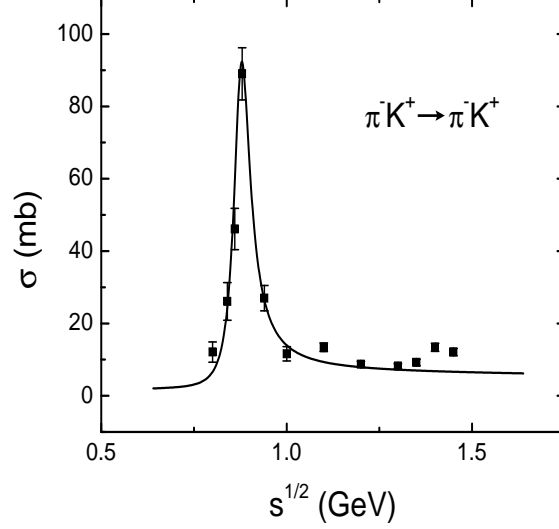


FIG. 3: Total elastic $\pi^- K^+ \rightarrow \pi^- K$ cross section as calculated in a meson-exchange model in Born approximation compared to experimental data from Ref. [26].

the form

$$q_0 \frac{dR_\gamma}{d^3q} = N \int \frac{d^3p_a}{2E_a(2\pi)^3} \frac{d^3p_b}{2E_b(2\pi)^3} \frac{d^3p_1}{2E_1(2\pi)^3} \frac{d^3p_2}{2E_2(2\pi)^3} \times (2\pi)^4 \delta^4(p_a + p_b - p_1 - p_2 - q) |\mathcal{M}_\gamma|^2 \frac{f(E_a)f(E_b)[1 \pm f(E_1)][1 \pm f(E_2)]}{2(2\pi)^3}, \quad (7)$$

where \mathcal{M}_γ is the corresponding scattering amplitude, $f(E_i) = 1/(e^{(E_i - \mu_i)/T} \pm 1) \equiv f_i$ are Fermi-Dirac or Bose-Einstein distribution functions (μ_i : chemical potential of hadron i), and the overall degeneracy factor N depends on the specific process. As elaborated in Appendix A, we rewrite the emission rate without further approximation as

$$q_0 \frac{dR_\gamma}{d^3q} = \frac{N}{16(2\pi)^{11}} \int |\mathbf{p}_a| dE_a d\phi_a \int |\mathbf{p}_b| dE_b \sin\theta_b d\theta_b d\phi_b \int |\mathbf{p}_1| dE_1 \sin\theta_1 d\theta_1 d\phi_1 f_a f_b [1 + f_1][1 + f_2] \frac{|\mathcal{M}_\gamma|^2}{\mathcal{A}} \quad (8)$$

where \mathcal{A} is given by

$$\mathcal{A} = |\varphi'(\cos\theta_a^r)| \quad (9)$$

and $\cos\theta_a^r$ is the root of the function $\varphi(\cos\theta_a)$,

$$\begin{aligned} \varphi(\cos\theta_a) = & (2|\mathbf{p}_a||\mathbf{p}_b|\sin\theta_b\cos\phi_a\cos\phi_b + 2|\mathbf{p}_a||\mathbf{p}_b|\sin\theta_b\sin\phi_a\sin\phi_b - 2|\mathbf{p}_a||\mathbf{p}_1|\sin\theta_1\cos\phi_a\cos\phi_1 \\ & - 2|\mathbf{p}_a||\mathbf{p}_1|\sin\theta_1\sin\phi_a\sin\phi_1)\sqrt{1 - \cos^2\theta_a} \\ & + (2|\mathbf{p}_a||\mathbf{p}_b|\cos\theta_b - 2|\mathbf{p}_a||\mathbf{p}_1|\cos\theta_1 - 2|\mathbf{p}_a||\mathbf{q}|\cos\theta_a \\ & + |\mathbf{p}_a|^2 + (\mathbf{p}_b - \mathbf{p}_1 - \mathbf{q})^2 - (E_a + E_b - E_1 - q_0)^2 + m_2^2) = 0. \end{aligned} \quad (10)$$

The main point of the present work is that the numerical evaluation of Eq. (8) goes beyond previous treatments [9, 22] by including the final state enhancement factors, $(1 + f_1) \times (1 + f_2)^1$, and by evaluating \mathcal{M}_γ beyond the soft photon approximation (SPA). The latter point is detailed in the following Section, where a summation over all possible processes for thermal photon Bremsstrahlung from π - π and π - K scattering is performed.

¹ The relevance of the final-state enhancement factors in hadronic phase of URHICs is further augmented by the build-up of substantial pion- and kaon-chemical potentials after chemical freezeout [27].

A. Amplitudes for Bremsstrahlung

The photon coupling to pseudoscalar and vector mesons can be implemented via a $U_{em}(1)$ gauge [7], rendering the interaction Lagrangian with electromagnetism as

$$\begin{aligned}
\mathcal{L} = & eA^\mu(\partial_\mu\vec{\pi} \times \vec{\pi})_3 + 2eg_{\sigma\pi\pi}\sigma A^\mu(\partial_\mu\vec{\pi} \times \vec{\pi})_3 - eg_{\rho\pi\pi}A_\mu[\vec{\pi} \times (\vec{\pi} \times \vec{\rho}^\mu)]_3 \\
& + e\{A^\mu(\partial_\mu\vec{\rho}^\nu \times \vec{\rho}_\nu)_3 + [(\partial_\mu A^\nu \vec{\rho}_\nu - A^\nu \partial_\mu \vec{\rho}_\nu) \times \vec{\rho}^\mu]_3 + [\vec{\rho}^\mu \times (A^\nu \partial_\mu \vec{\rho}_\nu - \partial_\mu A^\nu \vec{\rho}_\nu)]_3\} \\
& + ie[A^\mu(\vec{K}^{*\nu}Q\partial_\mu K_\nu^* - \partial_\mu \vec{K}^{*\nu}QK_\nu^*) + \vec{K}^{*\mu}Q(\partial_\mu A^\nu K_\nu^* - A^\nu \partial_\mu K_\nu^*) + (A^\nu \partial_\mu \vec{K}_\nu^* - \partial_\mu A^\nu \vec{K}_\nu^*)QK^{*\mu}] \\
& + ieA^\mu(\vec{K}Q\partial_\mu K - \partial_\mu \vec{K}QK) - eg_{\pi KK^*}A^\mu[\vec{K}^*(2\vec{\tau}Q - Q\vec{\tau})K + \vec{K}(2Q\vec{\tau} - \vec{\tau}Q)K^*] \cdot \vec{\pi} \\
& + eg_{\rho KK}A^\mu \vec{K}(\vec{\tau}Q + Q\vec{\tau})K \cdot \vec{\rho}_\mu,
\end{aligned} \tag{11}$$

where A^μ is the electromagnetic field, $Q=\text{diag}(1, 0)$ the charge operator, and the subscript ‘‘3’’ denotes the third component of isospin.

First, we consider the process for Bremsstrahlung of a photon via $\pi^a\pi^b \rightarrow \pi^1\pi^2\gamma$ scattering, based on the diagrams depicted in Fig. 1. In charge basis, this amounts to the following seven processes: $\pi^+\pi^- \rightarrow \pi^+\pi^-(\pi^0\pi^0)$, $\pi^+\pi^0 \rightarrow \pi^+\pi^0$, $\pi^-\pi^0 \rightarrow \pi^-\pi^0$, $\pi^0\pi^0 \rightarrow \pi^+\pi^-$, $\pi^+\pi^+ \rightarrow \pi^+\pi^+$ and $\pi^-\pi^- \rightarrow \pi^-\pi^-$, with a photon attached to each external or internal charged particle. E.g., the amplitude for the process $\pi^+\pi^- \rightarrow \pi^+\pi^-\gamma$ with a photon attached to a charged external pion in all possible ways reads

$$\begin{aligned}
\mathcal{M}^\mu = & eJ_a^\mu[\mathcal{M}_t(p_a - q, p_b, p_1, p_2) + \mathcal{M}_s(p_a - q, p_b, p_1, p_2)] \\
& + eJ_b^\mu[\mathcal{M}_t(p_a, p_b - q, p_1, p_2) + \mathcal{M}_s(p_a, p_b - q, p_1, p_2)] \\
& + eJ_1^\mu[\mathcal{M}_t(p_a, p_b, p_1 + q, p_2) + \mathcal{M}_s(p_a, p_b, p_1 + q, p_2)] \\
& + eJ_2^\mu[\mathcal{M}_t(p_a, p_b, p_1, p_2 + q) + \mathcal{M}_s(p_a, p_b, p_1, p_2 + q)],
\end{aligned} \tag{12}$$

where \mathcal{M}_s and \mathcal{M}_t are the amplitudes quoted in Sec. II. In the above,

$$J_{a,b}^\mu = \frac{-Q_{a,b}(2p_{a,b} - q)^\mu}{2p_{a,b} \cdot q}, \quad J_{1,2}^\mu = \frac{Q_{1,2}(2p_{1,2} + q)^\mu}{2p_{1,2} \cdot q} \tag{13}$$

are the electromagnetic currents with Q_i the charge of the pion in units of the proton charge. Electromagnetic gauge invariance furthermore requires the incorporation of contact diagrams with the photon attached to each proper vertex. In Appendix B we explicitly construct the pertinent amplitudes so that the total satisfies $q_\mu \cdot \mathcal{M}^\mu = 0$. For the processes with four-point vertices one arrives at

$$\begin{aligned}
\mathcal{M}_c^\mu = & \frac{4eg_{\sigma\pi\pi}^2 F[(p_b - p_2)^2](p_a + p_1)^\mu p_b \cdot p_2}{(p_b - p_2)^2 - m_\sigma^2 + im_\sigma\Gamma_\sigma} - \frac{4eg_{\sigma\pi\pi}^2 F[(p_a - p_1)^2]p_a \cdot p_1(p_b + p_2)^\mu}{(p_a - p_1)^2 - m_\sigma^2 + im_\sigma\Gamma_\sigma} \\
& - \frac{4eg_{\sigma\pi\pi}^2 (p_a - p_b)^\mu p_1 \cdot p_2}{(p_1 + p_2)^2 - m_\sigma^2 + im_\sigma\Gamma_\sigma} - \frac{4eg_{\sigma\pi\pi}^2 p_a \cdot p_b(p_1 - p_2)^\mu}{(p_a + p_b)^2 - m_\sigma^2 + im_\sigma\Gamma_\sigma} \\
& - \frac{2eg_{\rho\pi\pi}^2 F[(p_a - p_1)^2](p_a + p_1)^\mu}{(p_a - p_1)^2 - m_\rho^2 + im_\rho\Gamma_\rho} + \frac{2eg_{\rho\pi\pi}^2 F[(p_b - p_2)^2](p_b + p_2)^\mu}{(p_b - p_2)^2 - m_\rho^2 + im_\rho\Gamma_\rho} \\
& - \frac{2eg_{\rho\pi\pi}^2 (p_a - p_b)^\mu}{(p_a + p_b)^2 - m_\rho^2 + im_\rho\Gamma_\rho} - \frac{2eg_{\rho\pi\pi}^2 (p_1 - p_2)^\mu}{(p_1 + p_2)^2 - m_\rho^2 + im_\rho\Gamma_\rho}.
\end{aligned} \tag{14}$$

The same procedure of deriving the Bremsstrahlung amplitude, leading to Eqs. (12), can be applied to π - K scattering. The additional contact terms necessary to maintain gauge invariance are given by

$$\begin{aligned}
\mathcal{M}_c^\mu = & -\frac{2eg_{\rho\pi\pi}g_{\rho KK}F[(p_a - p_1)^2](p_a + p_1)^\mu}{(p_a - p_1)^2 - m_\rho^2 + im_\rho\Gamma_\rho} + \frac{2eg_{\rho\pi\pi}g_{\rho KK}F[(p_b - p_2)^2](p_b + p_2)^\mu}{(p_b - p_2)^2 - m_\rho^2 + im_\rho\Gamma_\rho} \\
& - \frac{4eg_{\pi KK^*}^2[(p_a - p_b)^\mu - (m_a^2 - m_b^2)(p_a + p_b)^\mu/m_{K^*}^2]}{(p_a + p_b)^2 - m_{K^*}^2 + im_{K^*}\Gamma_{K^*}} \\
& - \frac{4eg_{\pi KK^*}^2[(p_1 - p_2)^\mu - (m_1^2 - m_2^2)(p_1 + p_2)^\mu/m_{K^*}^2]}{(p_1 + p_2)^2 - m_{K^*}^2 + im_{K^*}\Gamma_{K^*}},
\end{aligned} \tag{15}$$

which completes the set of processes for $\pi K \rightarrow \pi K\gamma$.

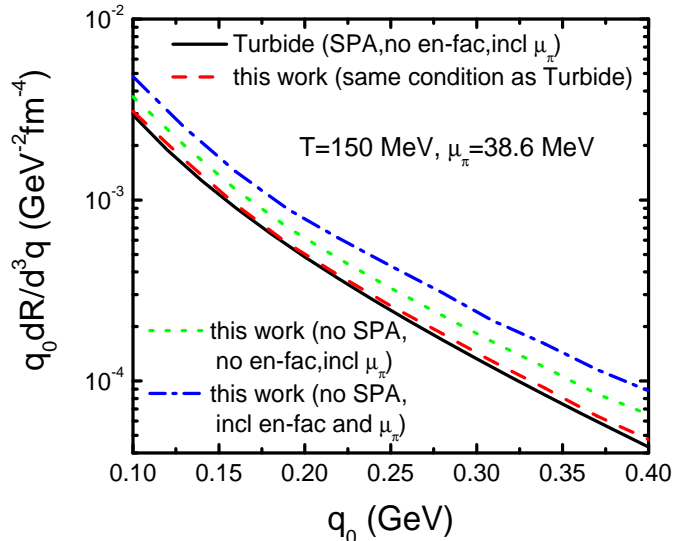


FIG. 4: Comparison of various approximations to the thermal photon rate for $\pi\pi \rightarrow \pi\pi\gamma$ reactions as a function of photon energy.

B. Soft Photon Emission Rates

With the amplitudes as specified in the previous section we now proceed to the results of the numerical integration of the thermal photon production rate, Eq. (8). In Fig. 4 we compare our new results for Bremsstrahlung off π - π scattering to earlier calculations. With the application to URHICs in mind, we choose medium conditions representing Pb - Pb collisions at full SPS energy, roughly half way through the hadronic evolution, corresponding to a temperature of $T = 150$ MeV and a pion chemical potential of $\mu_\pi \simeq 40$ MeV [11, 28]. When working in SPA and neglecting final-state Bose enhancement factors for the outgoing pions, our results closely coincide with computations by Turbide et al. [16, 17] (dashed vs. solid line in Fig. 4). When the SPA is relaxed, the rate is found to increase by about 25% at low energies ($q_0 = 0.1$ GeV) and close to 40% at higher energies ($q_0 \simeq 0.4$ GeV), see the short-dashed line in Fig. 4. Finally, when implementing the final-state Bose enhancement, the rate rises another $\sim 30\%$. Thus, the total increase of soft photon emission over previous computations amounts to 60-100%, which is quite appreciable and the main result of our paper.

In Fig. 5 we display the temperature evolution of the Bremsstrahlung rate from π - π scattering. The left panel includes pion-chemical potentials as estimated in Ref. [28] to preserve the pion (and kaon) number in the hadronic evolution of Pb - Pb collisions after chemical freezeout, parametrized by a linear increase with temperature (T in units of GeV),

$$\mu_\pi = \frac{0.2 - T}{1.05} \text{ GeV}, \quad \mu_K = 1.9 (0.175 - T) \text{ GeV} \quad (16)$$

(a small nonvanishing value of μ_π at chemical freezeout has been introduced to reproduce the measured pion-to-baryon ratio at full SPS energy; this is due to the somewhat limited number of resonances included in the equation of state in Ref. [28] which affects the pion yield via feeddown; it slightly overestimates (underestimates) the direct pion density at large (small) temperature, e.g., $e^{\mu_\pi/T} = 1.11$ at $T = 0.18$ GeV). When reducing the temperature from $T = 0.18$ GeV to 0.11 GeV, the decrease in rate is close to a factor of 10 at $q_0 = 0.1$ GeV but becomes a factor of ~ 15 at $q_0 = 0.4$ GeV, reflecting the larger slope at smaller T . This also entails an increasing weight of photon emission at lower energies toward later stages in the fireball evolution (note that increase in the hadronic fireball volume between chemical ($T_c = 0.175$ GeV) and thermal freezeout ($T \simeq 0.110$ GeV) is about a factor of ~ 6 , implying that the yield of Bremsstrahlung photons is rather sensitive to the late stages of the fireball lifetime). In the right panel of Fig. 5, the pion-chemical potentials are set to zero: the decrease compared to the $\mu_\pi \neq 0$ results amounts to slightly more than a fugacity factor squared, $e^{2\mu_\pi/T}$ (as one would naively expect for $\pi\pi$ annihilation), mostly due to the final-state enhancement factors. Finally, a comparison to the hadronic rate calculations of Ref. [11] reveals that π - π Bremsstrahlung as computed here exceeds previously dominant baryonic contributions by close to a factor of 2 at $q_0 = 0.2$ GeV, and is smaller by a factor of 2 at $q_0 = 0.4$ GeV.

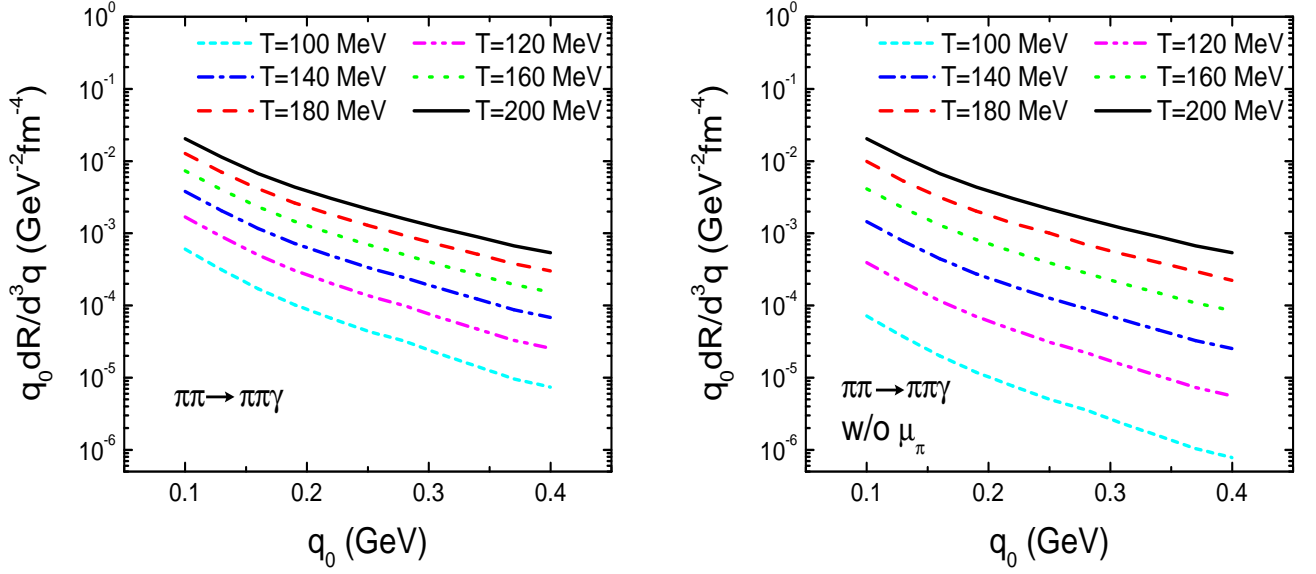


FIG. 5: Thermal photon emission rate from Brehmsstrahlung via $\pi\pi \rightarrow \pi\pi\gamma$ reactions as a function of photon energy at different temperatures. The left panel includes pion chemical potentials appropriate for $Pb(158 \text{ AGeV})\text{-}Pb$ collisions while in the right panel $\mu_\pi = 0$.

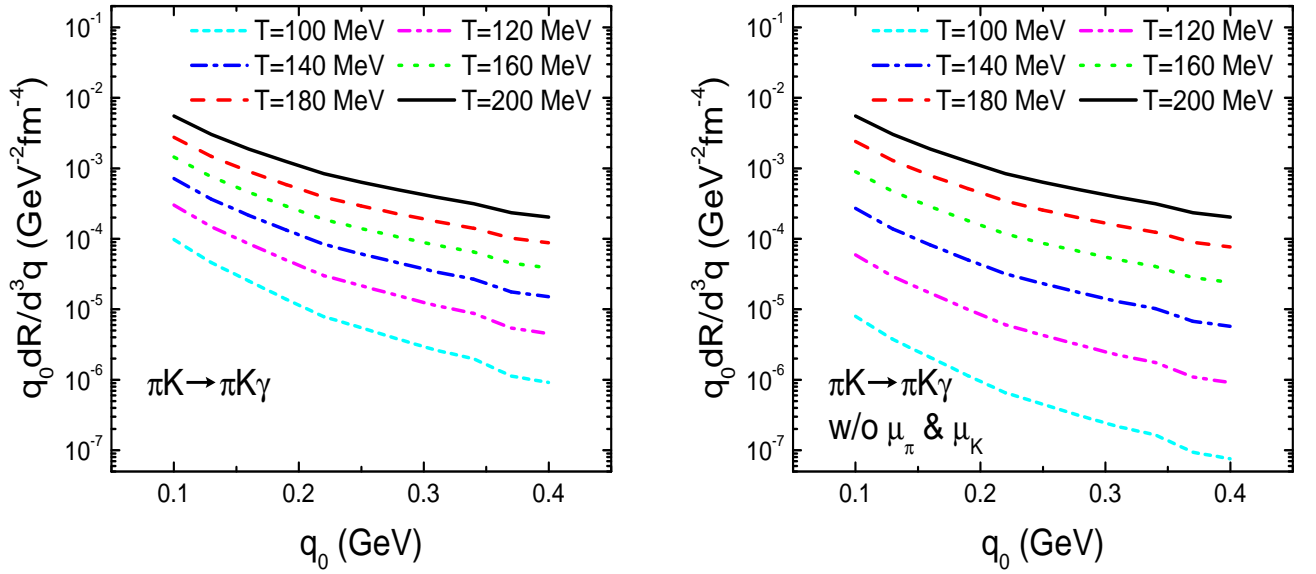


FIG. 6: Thermal photon Brehmsstrahlung emission rate from $\pi K \rightarrow \pi K\gamma$ reactions as a function of photon energy at different temperatures. The left panel includes pion- and kaon-chemical potentials according to Eq. (16), while in the right panel $\mu_\pi = \mu_K = 0$.

Turning to γ radiation off elastic π - K scattering (Fig. 6), we find the emission rate to be at the $\sim 20\%$ level of the one from $\pi\pi$ scattering, which essentially reflects the experimentally observed K/π ratio. Since π - π scattering could provide the dominant contribution to the overall low-energy yield (i.e., in the low- q_t spectra of URHICs), the strangeness component may be significant. Also, the role of the kaon-chemical potential, μ_K , is equally relevant for maintaining a substantial emission rate for π - K scattering toward lower temperatures (compare left and right panels of Fig. 6) as is μ_π for π - π scattering.

Additional sources of photon Brehmsstrahlung in meson-meson scattering have been examined in Ref. [12] within the soft photon approximation. At a temperature of $T = 200 \text{ MeV}$ and at low energies, $q_0 \leq 0.5 \text{ GeV}$, Brehmsstrahlung off $\pi\pi$ scattering was found to exceed the one off πK scattering by about a factor of ~ 5 , roughly in line with our results (we find a factor of ~ 3 -4). Furthermore, $\pi\rho \rightarrow \pi\rho\gamma$ processes were found to give a low-energy photon yield comparable to $\pi K \rightarrow \pi K\gamma$, while other channels (KK , $K\rho$, πK^*) are suppressed by an order of magnitude or more. However,

at lower temperatures, the rate for $\pi\rho \rightarrow \pi\rho\gamma$ will decrease faster than the one for $\pi K \rightarrow \pi K\gamma$, due to thermal suppression caused by the larger ρ -mass relative to the kaon mass (e.g., at $T=120$ MeV we estimate the relative suppression of former relative to the latter to be a factor of ~ 1.7 , which includes the effects of the meson-chemical potentials; without the latter, the suppression will be larger). $\pi\eta$ channels are suppressed relative to πK , due to the mass and small degeneracy of the η , which, in addition, is electrically neutral. Thus, for meson-meson Bremsstrahlung in heavy-ion collisions, one can expect all channels other than $\pi\pi$ and πK to contribute on the $\sim 20\%$ level or less.

Finally, let us compare the absolute magnitude of our rates to other calculations available in the literature. For $T = 200$ MeV, our $\pi\pi \rightarrow \pi\pi\gamma$ rate for $\mu_\pi = 0$ closely follows the result of Ref. [9] (obtained in SPA), only that our rate is a factor 2 larger. This is precisely the enhancement we deduced from Fig. 4 as being due to the improvements in the present work. On the other hand, our results do not compare well with those found in Ref. [12], Fig. 3, where at $q_0 = 250$ MeV and $T = 200$ MeV the rates are larger by at least a factor of ~ 2 , despite being evaluated in SPA. The origin of this discrepancy deserves further study.

IV. FURTHER UNCERTAINTIES IN THE EMISSION RATES

Before we apply our Bremsstrahlung rate to estimate low-energy photon production in heavy-ion reactions at the SPS, we would like to illustrate two additional uncertainties in the determination of the emission rates. The first one relates to the well-known Landau-Pomeranchuk-Migdal (LPM) interferences, while the second one concerns possible medium effects on the meson exchanges which build up the meson-meson interactions.

A. Landau-Pomeranchuk-Migdal Effect

When the formation time of the emitted photon, $\tau_{form} \sim 1/q_0$, becomes of the same order as the time between subsequent π - π collisions, τ_π^{coll} , coherence effects are expected to become important (LPM effect [29]). For soft photon and dilepton production in a dense hadronic gas, the LPM interference has been studied in Refs. [8, 20, 21]. Here, we put these estimates into context with our updated rate calculations. First, we recall the expression derived in Ref. [20], where the LPM effect was implemented in SPA resulting in a differential cross section of photon production off π - π scattering as

$$q_0 \left\langle \frac{d\sigma^\gamma}{d^3q} \right\rangle = \sigma_{\pi\pi} \frac{2\alpha}{(2\pi)^2} \left\langle v^2 \frac{(1 - \cos^2\theta)}{a^2 + q_0^2(1 - v\cos\theta)^2} \right\rangle. \quad (17)$$

$\langle \cdot \rangle$ indicates averaging over the time between successive collisions and over all the velocities after the collision (for simplicity, we choose an average velocity $v = 0.5c$), $\sigma_{\pi\pi}$ denotes the elastic π - π cross section (which factorizes in SPA) and $1/a = \tau_\pi^{coll} = 1/\Gamma_\pi$ is the pion collision time (or inverse scattering width). The latter, in turn, depends on the hadron densities and pertinent pion cross sections, schematically given by

$$\Gamma_\pi = \sum_h n_h(T, \mu_h) \sigma_{\pi h} v_{rel}, \quad (18)$$

where the summation is, in principle, over all hadrons in the heat bath ($h = \pi, K, N, \Delta, \dots$; v_{rel} : relative velocity between π and h). For a selfconsistently calculated pion gas at $(T, \mu_\pi) = (150, 0)$ MeV with realistic $\pi\pi$ interactions [30], one finds $\tau_\pi^{coll} \simeq 6$ fm/c, while a hot $\pi N\Delta$ gas representative for SPS conditions leads to $\tau_\pi^{coll} \simeq 2$ fm/c [31]. In Fig. 7 we used both values to bracket the uncertainty in the suppression of low-energy photons, by plotting the ratio of Eq. (17) to the incoherent limit ($a = 0$). For $\tau_\pi^{coll} = 6$ fm/c, the quenching factor is rather small reducing the photon emission rate by no more than 15% even at the smallest energies considered here, $q_0 = 100$ MeV. This is consistent with Ref. [21] where a slightly different coherence factor has been derived, amounting to a multiplication of the incoherent rate by $[(q_0\tau)^2/(1 + (q_0\tau)^2)]^2$; for $\tau_\pi^{coll} = 6$ fm/c and $q_0 = 100$ MeV the latter turns out to be 0.81. However, for $\tau_\pi^{coll} = 2$ fm/c and $q_0 = 100$ MeV, collision and formation time are of comparable magnitude, and the quenching factor becomes substantial, between 0.4 and 0.25 according to the two ways of estimating it.

B. Schematic Estimate of Medium Effects

When hadrons are embedded into a hot and dense medium, their vacuum properties (mass and width) are expected to change, which is encoded in pertinent spectral functions,

$$A_h(k_0, k) = -2 \text{Im} D_h(k^2) = -2 \text{Im} \left(\frac{1}{k^2 - m_h^2 - \Sigma_h(k_0, k)} \right), \quad (19)$$

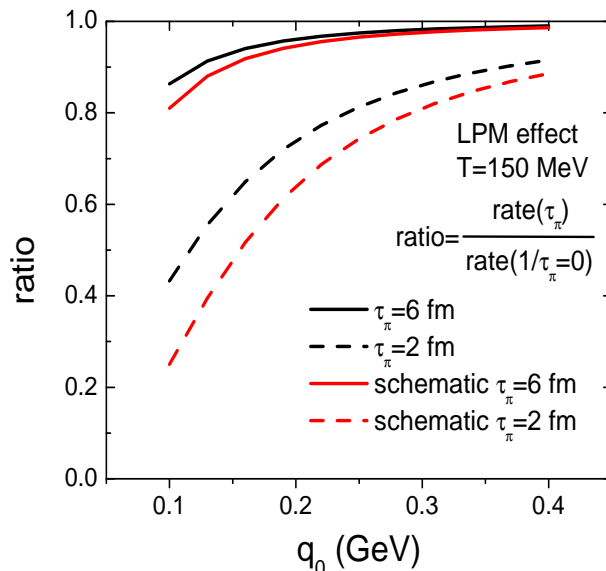


FIG. 7: Influence of the LPM effect on thermal photon bremsstrahlung from $\pi\pi$ scattering at $T = 150$ MeV.

where $\Sigma_h(k_0, k)$ is the self-energy of meson h as induced by interactions with the surrounding matter particles. For the present purpose, the relevant mesons are the ρ and the “ σ ” which figure into the meson-exchange propagators in the amplitudes (since we work in Born approximation, no explicit pion propagators appear). Dilepton spectra in heavy-ion collisions have revealed ample evidence that the in-medium ρ -meson spectral function is substantially modified. While the low-mass enhancement observed by CERES/NA45 in $Pb(158 \text{ AGeV})\text{-Au}$ collisions [32] is compatible with both the assumption of a dropping ρ -mass and a broadening as predicted by hadronic many-body theory [28], more recent NA60 dimuon spectra [33] clearly favor the latter [34]. Concerning the “ σ ” meson, 2-pion production experiments off nuclei [35, 36] indicate substantial medium effects as well, in terms of an enhancement near the two-pion threshold which increases with nuclear mass number A . Whether this is due to a dropping “ σ ”-meson mass [37] or hadronic many-body effects [38] (or both), is not clear at present. At finite temperature, the (the approach to) chiral symmetry restoration (implying degeneracy of π - and σ - spectral functions), is suggestive for a σ -mass approaching the pion mass [39]. It is therefore desirable to investigate to what extent Bremsstrahlung off π - π scattering is sensitive to modifications of “ σ ” and ρ mesons. Previous studies along these lines [40, 41, 42] have mostly addressed hadronic photon emission at higher energies (in connection with a dropping ρ mass).

In light of the above, we here focus on the effects of a reduced σ -mass on low-energy photon emission. We will not address changes in the ρ -meson properties, as a simple dropping mass appears to be ruled out while a consistent implementation of changes in the width in the propagator requires accounting for the pertinent processes in the photon production rate as well (for the same reason, we do not consider width changes in the σ -propagator).

When recalculating photon Bremsstrahlung off π - π scattering by reducing the mass of the σ meson to $m_\sigma = 0.45$ GeV (as compared to 0.525 GeV before), the thermal emission rate barely changes, cf. Fig. 8. This can be readily understood by recalling in the elastic π - π cross section the σ -meson contribution plays a minor role, cf. right panel in Fig. 2. Nevertheless, the smallness of the effect when dropping the σ mass by $\sim 15\%$ is not necessarily expected, but forces us to conclude that low-energy thermal photon spectra are not sensitive to (partial) chiral symmetry restoration in the scalar channel (for completeness we state that the rate of low-energy photon production increases by $\sim 25\%$ if one were to reduce the ρ -meson mass from its vacuum value of 0.77 GeV to 0.65 GeV).

V. PHOTON SPECTRA IN HEAVY-ION COLLISIONS

We now apply our Bremsstrahlung rates to the calculation of photon spectra at low transverse momentum in central $Pb(158 \text{ AGeV})\text{-Pb}$ collisions at SPS. We supplement the spectra with the baseline results of Ref. [11]² and

² To avoid double counting, we have removed the contributions from $\rho \rightarrow \pi\pi\gamma$, $\pi\pi \rightarrow \rho\gamma$, $K^* \rightarrow K\pi\gamma$ and $\pi K \rightarrow K^*\gamma$ from the rates of Ref. [11], as they are part of the $\pi\pi \rightarrow \pi\pi\gamma$ and $\pi\pi \rightarrow \pi\pi\gamma$ processes when using full $\pi\pi$ and πK cross sections; the latter include

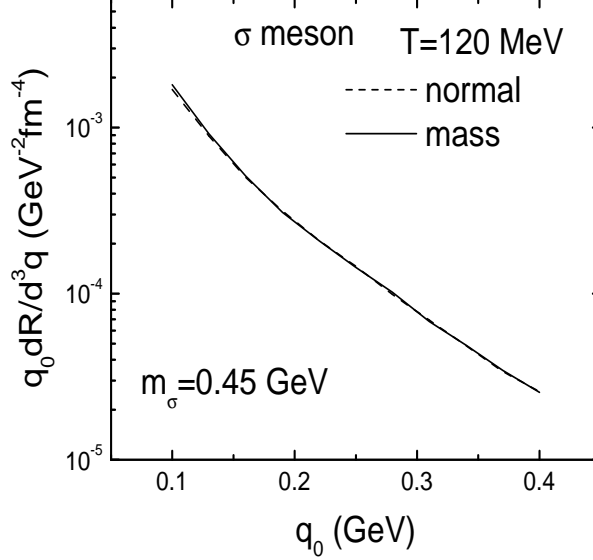


FIG. 8: In-medium effects on thermal photon production implemented by a dropping “ σ ”-meson mass in Bremsstrahlung off π - π scattering. Dashed ($m_\sigma = 0.525$ GeV) and solid line ($m_\sigma = 0.45$ GeV) are almost indistinguishable due to the minor role of “ σ ”-exchange in the total elastic π - π cross section at low energy.

compare the total to the recent WA98 data [15]. As in Ref. [11], the folding of the thermal emission rates over the space-time evolution is performed with the help of an expanding fireball evolution which has been parametrized to reflect basic features of hydrodynamic models. With a hadronic resonance-gas equation of state (with chemical freezeout at $(\mu_N^{ch}, T_{ch}) = (250, 175)$ MeV) and a participant-nucleon number of $N_{part} = 340$ to represent the 10% most central collisions, the fireball volume at chemical freezeout is fixed to approximately reproduce the observed hadron multiplicities (after chemical freezeout, the evolution is constructed using entropy and baryon-number conservation, as well as meson-chemical potentials to preserve the correct hadron ratios). After averaging over the appropriate rapidity interval of the WA98 acceptance the thermal photon spectra follow as

$$q_0 \frac{dN}{d^3q}(q_t) = \frac{1}{\Delta y} \int_{y_{min}}^{y_{max}} dy \int d\tau V_{FB}(\tau) q_0 \frac{dR^\gamma}{d^3q} \quad (20)$$

with $y_{min} = 2.35$ and $y_{max} = 2.95$ ($\Delta y = 0.6$). The fireball volume is taken to evolve with proper time as

$$V_{FB}(\tau) = \frac{1}{2} \pi (z_0 + v_{z,0} \tau + \frac{1}{2} a_z \tau^2) (r_{T,0} + \frac{1}{2} a_T \tau^2)^2 \quad (21)$$

with $z_0 = 1.8$ fm (corresponding to a formation time of 1 fm/c and translating into an average initial temperature of $T_0 = 205$ MeV), $r_{T,0} = 6.25$ fm, $a_z = a_T = 0.045$ c²/fm, and $v_z = 0.6c$ (note that only half of the total fireball volume must be used to reproduce the correct dN_{ch}/dy). QGP and mixed phase are completed after $\tau_H \simeq 4.46$ fm/c and thermal freezeout is assumed at $\tau_{fo} = 13$ fm/c (plus one extra fm/c to allow for strong resonance decays). The numerically inferred temperature evolution in the hadronic phase can be conveniently parametrized as

$$T(\tau) = \frac{1}{c_1 + c_2 R(\tau)} \text{GeV} , \quad (22)$$

with $c_1 = 1.3$, $c_2 = 0.639/\text{fm}$, and a “radius”

$$R(\tau) = \left(\frac{3}{4\pi} V_{FB}(\tau) \right)^{\frac{1}{3}} . \quad (23)$$

(unstable) ρ and K^* mesons which should not be counted twice.

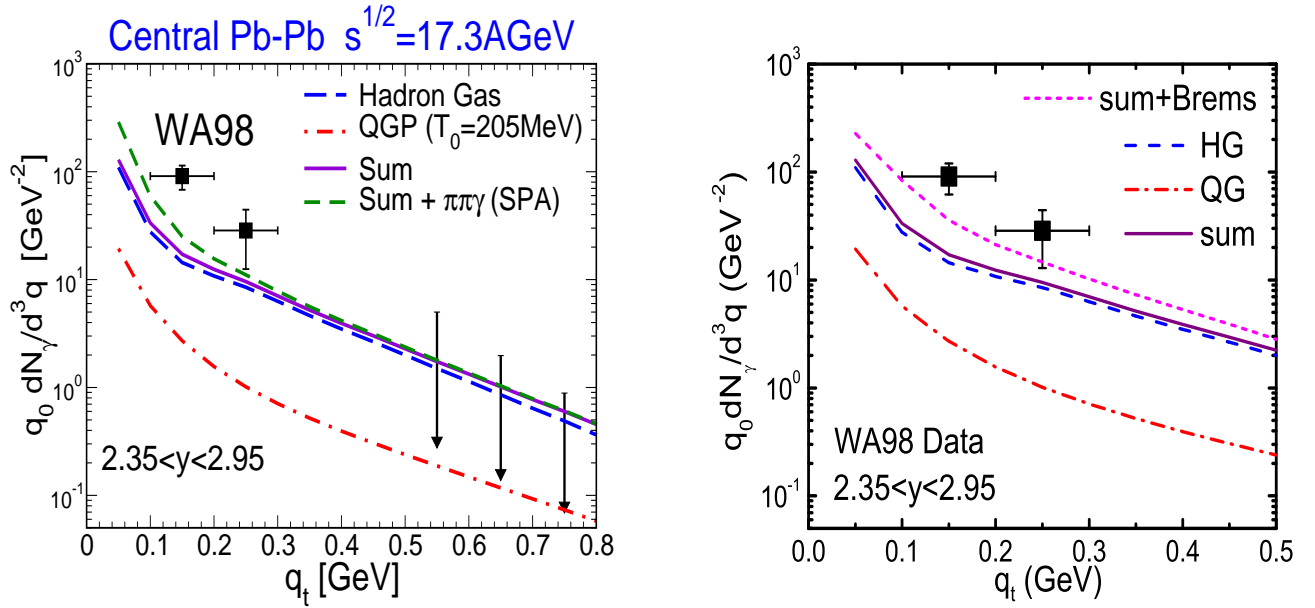


FIG. 9: Direct low- q_t photon spectra as measured in central $Pb-Pb$ collisions at SPS [15] compared to thermal emission spectra from an expanding thermal fireball with QGP and hadronic phases [11]. In the left panel (taken from Refs. [16, 17]) QGP [43] (dash-dotted line) and hadron gas (HG) emission [11] (dashed line, without meson-meson Brehmsstrahlung) add up to the solid line, while the upper dashed line additionally includes an estimate [16] of Brehmsstrahlung off $\pi-\pi$ scattering in the soft-photon approximation (SPA) and without final-state Bose enhancement factors, representing the rate depicted by the solid line in Fig. 4 (the contributions from $\rho \rightarrow \pi\pi\gamma$ decays in the HG rates of Ref. [11] have been removed to avoid double counting). The downward arrows represent 90% upper confidence limits set by WA98 in an earlier measurement [14]. The curves in the right panel are as in the left panel except that the upper dashed line now includes the improved rates from elastic $\pi-\pi$ and $\pi-K$ Brehmsstrahlung (without SPA, including final-state Bose enhancement and with a similar caveat on double counting as in the left panel, cf. footnote 2).

Parameterizations of the numerically computed Brehmsstrahlung rates along the temperature-chemical potential trajectory used here (as well as separately in q_0 , T and μ_π) are quoted in Appendix C.

In Fig. 9 we summarize our results for direct photon spectra in central $Pb(158 \text{ AGeV})-Pb$ in comparison to the low- q_t data of WA98 [15] at the CERN-SPS. As noted in the introduction, these data are extracted via a photon HBT method requiring an assumption on the emission source size implying an extra (systematic) error of the data (in addition, strictly speaking, the weighted average of each data point does not correspond to the center of the transverse-momentum bin, but is shifted to somewhat smaller q_t , due to the rather sharp increase of the yield toward lower q_t). The left panel of Fig. 9 reproduces the previous calculations for QGP and hadron gas emission of Ref. [11] (lower three curves), which are in good agreement with earlier WA98 spectra at $q_t \geq 1.5 \text{ GeV}$, but significantly underestimate the low-momentum data at $q_t = 0.1 - 0.3 \text{ GeV}$. This is still true upon inclusion of Brehmsstrahlung off $\pi-\pi$ scattering [16, 17] treated in SPA and without final-state Bose enhancement, even though this contribution is noticeable. However, if the improved Brehmsstrahlung rates from $\pi-\pi$ and $\pi-K$ interactions are employed, the discrepancy is reduced appreciably, see right panel of Fig. 9 (note that the Brehmsstrahlung yield decreases faster with energy than the other hadronic contributions, thereby not upsetting the agreement of the previous calculations with the experimental spectra (upper limits) at higher energies). These findings are presumably to be considered as an upper limit since at this point we do not account for LPM suppression effects as discussed in Sec. IV A. The thermal low- q_t photon yield is furthermore found to approximately scale with the fireball lifetime, which reiterates the importance of the later hadronic stages (on the other hand, the sensitivity to transverse flow effects is small).

We also note that baryon-induced effects, which enter through a medium modified ρ spectral function [28] carried to the photon point and which dominate the contribution labeled “HG” at the depicted momenta, are appreciable (at the 30-60% level in the range $q_t = 0.1 - 0.3 \text{ GeV}$). Besides resonance decays (e.g., $\Delta, N(1520) \rightarrow N\gamma$), these include Brehmsstrahlung from $\pi-N$, $N-N$, and $N-\Delta$ interactions (as following from πNN^{-1} and $\pi\Delta N^{-1}$ excitations in the pion cloud of the ρ -meson), which have been constrained by (the inverse process of) photoabsorption on the nucleon and nuclei [44]. In Ref. [10], similar contributions were claimed to be smaller.

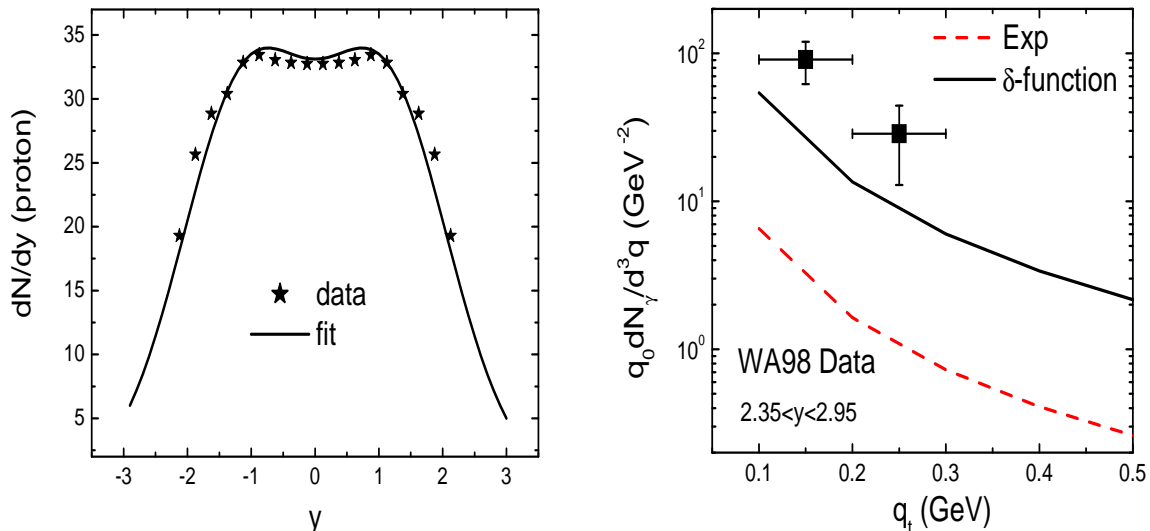


FIG. 10: Left panel: two-Gaussian fit (with centers at $y_0 = \pm 1.1$ and width $\sigma_y = 1.0$) to the experimental proton rapidity distributions [47] in central $Pb(158 \text{ AGeV})-Pb$. Right panel: coherent photon spectra from $Pb-Pb$ collisions at SPS using final-state proton rapidity distributions from experiment (dashed line) or δ -functions centered at $y_{P,T} = \pm 0$ (solid line), compared to the experimental data [15].

VI. COHERENT EMISSION FROM HEAVY-ION COLLISIONS

Another source of soft direct photons in heavy-ion collisions that we would like to study here is (nonthermal) Bremsstrahlung emission due to coherent radiation off the protons within the incoming nuclei [45, 46]. In the long-wave length limit, $\lambda_\gamma = 2\pi/q \gg D$ (q : photon 3-momentum, $D \simeq 10 \text{ fm}$: typical system size), phase interferences are suppressed and the radiation can be assessed via the rapidity shift that the protons undergo from the initial nuclei to the finally observed distribution. Including both target and projectile, and for central collisions, one finds the following form of the photon spectrum [45, 46],

$$q_0 \frac{dN_\gamma}{d^3q} = \frac{\alpha_{em}}{4\pi^2 q_0^2} \left| \int dy \left\{ \frac{dN}{dy} \Big|_P \left[\frac{v \sin\theta}{1 - v \cos\theta} - \frac{v_P \sin\theta}{1 - v_P \cos\theta} \right] + \frac{dN}{dy} \Big|_T \frac{v \sin\theta}{1 - v \cos\theta} \right\} \right|^2 \quad (24)$$

where v_P is the beam velocity, $y = \tanh^{-1} v$ is the final-state (FS) proton rapidity, and

$$\frac{dN}{dy} \Big|_P \quad \text{and} \quad \frac{dN}{dy} \Big|_T \quad (25)$$

are the pertinent FS rapidity distributions for projectile and target nuclei, respectively. The latter can be reasonably well fitted to experimental data [47] using two Gaussians, cf. left panel of Fig. 10. In the right panel of Fig. 10 we summarize our results for coherent emission from the longitudinal deceleration of the incoming protons. With realistic final rapidity distributions (dashed line) the photon yield constitutes only a few percent of the WA98 low-energy data, which presumably is an upper limit since already for $q_0 = 0.1 \text{ GeV}$, the pertinent photon wavelength, $\lambda_\gamma \simeq 12 \text{ fm}$, is of the order of the system size rendering phase variations (interference) potentially relevant. Even with the extreme assumption of δ -function like proton rapidity distributions at $y_{P,T} = 0$ (full stopping), the coherent emission yield falls significantly short of the data. We thus conclude that this mechanism cannot be at the origin of the observed enhancement over previous predictions [11].

VII. SUMMARY AND DISCUSSION

In this article we have revisited the problem of soft photon production from hadronic matter which has recently received renewed interest by the observation of a large excess by the WA98 collaboration in central $Pb-Pb$ collisions at the CERN-SPS. Earlier predictions using two-body mesonic and baryon-induced thermal photon production significantly underestimated these data. We have focused on a more elaborate re-evaluation of Bremsstrahlung from

meson-meson interactions. Based on a $U_{\text{em}}(1)$ -gauged meson-exchange model for elastic π - π and π - K scattering (in Born approximation), our main improvement over previous calculations consists of a full numerical treatment of the collision integral which goes beyond the commonly employed soft-photon approximation and allows for the inclusion of final-state Bose enhancement factors. We have explicitly constructed pertinent contact interactions to preserve electromagnetic gauge invariance of the underlying Bremsstrahlung amplitude. The combined effect of the two improvements amounts to an increase of the thermal π - π Bremsstrahlung rate by up to a factor of 2 at low photon energies ($q_0 = 0.1 - 0.5$ GeV), while π - K scattering adds another $\sim 20\%$ (essentially reflecting the K/π ratio in the hadronic gas). As a consequence, meson-meson Bremsstrahlung becomes the dominant thermal photon source at low energies. When combined with previous rate calculations, the convolution over a standard thermal fireball evolution reduces previously found discrepancies with the low-momentum WA98 data. This comparison, however, does not include the LPM effect, which we have estimated to suppress the soft emission rate by up to several tens of percent. We have furthermore shown that the Bremsstrahlung rates are rather insensitive to medium effects on the " σ "-meson in form of a reduced mass, due to the fact that the elastic π - π cross section is dominated by (s -channel) ρ exchange. We finally studied the possibility of coherent Bremsstrahlung induced by rapidity shifts of the incoming projectile and target protons. When using realistic final-state distributions, we have found this contribution to be essentially negligible.

While our investigations suggest that thermal emission from hadronic matter might be at the origin of the low- q_t WA98 enhancement, more work is required to quantify the theoretical estimates, e.g. by merging medium effects on the ρ -meson (as implicit in rate estimates using in-medium spectral functions) with the newly computed Bremsstrahlung rates, as well as by explicit implementations of the LPM effect. In addition, an experimental confirmation of the observed enhancement, e.g. at the Relativistic Heavy-Ion Collider (RHIC), would be very illuminating.

Acknowledgments

We gratefully acknowledge discussions with C. Gale and S. Turbide in the early stages of this work, and for supplying us with the Bremsstrahlung rates used in the left panel of Fig. 9. We also wish to thank Che-Ming Ko and Hendrik van Hees for helpful discussions. This work was supported in part by a U.S. National Science Foundation CAREER award under grant PHY-0449489.

APPENDIX A: EVALUATION OF THE BREMSSTRAHLUNG PHASE SPACE INTEGRAL

In this appendix, we derive the expressions for the photon emission rate as used in Sec. III. Starting from the kinetic theory expression, Eq. (7) in the main text, for $\pi + \pi \rightarrow \pi + \pi + \gamma$,

$$q_0 \frac{dR^\gamma}{d^3q} = N \int \frac{d^3p_a}{2E_a(2\pi)^3} \frac{d^3p_b}{2E_b(2\pi)^3} \frac{d^3p_1}{2E_1(2\pi)^3} \frac{d^3p_2}{2E_2(2\pi)^3} \times (2\pi)^4 \delta^4(p_a + p_b - p_1 - p_2 - q) |\mathcal{M}_i|^2 \frac{f_a(E_a) f_b(E_b) [1 + f_1(E_1)] [1 + f_2(E_2)]}{2(2\pi)^3}, \quad (\text{A1})$$

we perform the integrations over the energy-momentum conserving delta function to obtain

$$\begin{aligned} q_0 \frac{dR^\gamma}{d^3q} &= \frac{N}{16(2\pi)^{11}} \int \frac{d^3p_a}{E_a} \frac{d^3p_b}{E_b} \int \frac{d^3p_1}{E_1} f_1 f_2 [1 + f_3] [1 + f_4] \\ &\quad \times |\mathcal{M}_i|^2 \delta((E_a + E_b - E_1 - q_0)^2 - (\mathbf{p}_a + \mathbf{p}_b - \mathbf{p}_1 - \mathbf{q})^2 - m_4^2) \\ &= \frac{N}{16(2\pi)^{11}} \int |\mathbf{p}_a| dE_a d\Omega_a \int |\mathbf{p}_b| dE_b d\Omega_b \int |\mathbf{p}_1| dE_1 d\Omega_1 f_1 f_2 [1 + f_3] [1 + f_4] \\ &\quad \times |\mathcal{M}_i|^2 \delta((E_a + E_b - E_1 - q_0)^2 - (\mathbf{p}_a + \mathbf{p}_b - \mathbf{p}_1 - \mathbf{q})^2 - m_4^2). \end{aligned} \quad (\text{A2})$$

We evaluate this equation by the Monte Carlo method, choosing the coordinates for each particle as follows,

$$\begin{aligned} p_a &= (E_a, |\mathbf{p}_a| \sin\theta_a \cos\phi_a, |\mathbf{p}_a| \sin\theta_a \sin\phi_a, |\mathbf{p}_a| \cos\theta_a), \\ p_b &= (E_b, |\mathbf{p}_b| \sin\theta_b \cos\phi_b, |\mathbf{p}_b| \sin\theta_b \sin\phi_b, |\mathbf{p}_b| \cos\theta_b), \\ p_1 &= (E_1, |\mathbf{p}_1| \sin\theta_1 \cos\phi_1, |\mathbf{p}_1| \sin\theta_1 \sin\phi_1, |\mathbf{p}_1| \cos\theta_1), \\ q &= (q_0, 0, 0, |\mathbf{q}|), \\ p_2 &= p_a + p_b - p_1 - q, \end{aligned} \quad (\text{A3})$$

with

$$E_i = \sqrt{m_i^2 + \mathbf{p}_i^2} \quad (i = a, b, 1, 2, q). \quad (\text{A4})$$

Thus, Eq. (A2) can be rewritten as

$$q_0 \frac{dR^\gamma}{d^3q} = \frac{N}{16(2\pi)^{11}} \int |\mathbf{p}_a| dE_a \sin\theta_a d\theta_a d\phi_a \int |\mathbf{p}_b| dE_b \sin\theta_b d\theta_b d\phi_b \int |\mathbf{p}_1| dE_1 \sin\theta_1 d\theta_1 d\phi_1 f_1 f_2 [1 + f_3][1 + f_4] \times |\mathcal{M}_i|^2 \delta((E_a + E_b - E_1 - q_0)^2 - (\mathbf{p}_a + \mathbf{p}_b - \mathbf{p}_1 - \mathbf{q})^2 - m_2^2). \quad (\text{A5})$$

In the argument of the delta function, one has

$$\begin{aligned} (\mathbf{p}_a + \mathbf{p}_b - \mathbf{p}_1 - \mathbf{q})^2 &= |\mathbf{p}_a|^2 + 2\mathbf{p}_a \cdot \mathbf{p}_b - 2\mathbf{p}_a \cdot \mathbf{p}_1 - 2\mathbf{p}_a \cdot \mathbf{q} + (\mathbf{p}_b - \mathbf{p}_1 - \mathbf{q})^2 \\ &= 2|\mathbf{p}_a||\mathbf{p}_b|\sin\theta_a\sin\theta_b\cos\phi_a\cos\phi_b + 2|\mathbf{p}_a||\mathbf{p}_b|\sin\theta_a\sin\theta_b\sin\phi_a\sin\phi_b + 2|\mathbf{p}_a||\mathbf{p}_b|\cos\theta_a\cos\theta_b \\ &\quad - 2|\mathbf{p}_a||\mathbf{p}_1|\sin\theta_a\sin\theta_1\cos\phi_a\cos\phi_1 - 2|\mathbf{p}_a||\mathbf{p}_1|\sin\theta_a\sin\theta_1\sin\phi_a\sin\phi_1 - 2|\mathbf{p}_a||\mathbf{p}_1|\cos\theta_a\cos\theta_1 \\ &\quad - 2|\mathbf{p}_a||\mathbf{q}|\cos\theta_a + |\mathbf{p}_a|^2 + (\mathbf{p}_b - \mathbf{p}_1 - \mathbf{q})^2. \end{aligned} \quad (\text{A6})$$

Upon integrating over θ_a , we arrive at

$$q_0 \frac{dR^\gamma}{d^3q} = \frac{N}{16(2\pi)^{11}} \int |\mathbf{p}_a| dE_a d\phi_a \int |\mathbf{p}_b| dE_b \sin\theta_b d\theta_b d\phi_b \int |\mathbf{p}_1| dE_1 \sin\theta_1 d\theta_1 d\phi_1 f_1 f_2 [1 + f_3][1 + f_4] \frac{|\mathcal{M}_i|^2}{\mathcal{A}} \quad (\text{A7})$$

with

$$\mathcal{A} = |\varphi'(\cos\theta_a^r)|. \quad (\text{A8})$$

In the above, $\cos\theta_a^r$ is the root of function $\varphi(\cos\theta_a)$,

$$\begin{aligned} \varphi(\cos\theta_a) &= (2|\mathbf{p}_a||\mathbf{p}_b|\sin\theta_b\cos\phi_a\cos\phi_b + 2|\mathbf{p}_a||\mathbf{p}_b|\sin\theta_b\sin\phi_a\sin\phi_b - 2|\mathbf{p}_a||\mathbf{p}_1|\sin\theta_1\cos\phi_a\cos\phi_1 \\ &\quad - 2|\mathbf{p}_a||\mathbf{p}_1|\sin\theta_1\sin\phi_a\sin\phi_1)\sqrt{1 - \cos^2\theta_a} \\ &\quad + (2|\mathbf{p}_a||\mathbf{p}_b|\cos\theta_b - 2|\mathbf{p}_a||\mathbf{p}_1|\cos\theta_1 - 2|\mathbf{p}_a||\mathbf{q}|\cos\theta_a \\ &\quad + |\mathbf{p}_a|^2 + (\mathbf{p}_b - \mathbf{p}_1 - \mathbf{q})^2 - (E_a + E_b - E_1 - q_0)^2 + m_2^2) = 0. \end{aligned} \quad (\text{A9})$$

with

$$\begin{aligned} (\mathbf{p}_b - \mathbf{p}_1 - \mathbf{q})^2 &= |\mathbf{p}_b|^2 + |\mathbf{p}_1|^2 + |\mathbf{q}|^2 - 2|\mathbf{p}_b||\mathbf{p}_1|\sin\theta_b\sin\theta_1\cos\phi_b\cos\phi_1 - 2|\mathbf{p}_b||\mathbf{p}_1|\sin\theta_b\sin\theta_1\sin\phi_b\sin\phi_1 \\ &\quad - 2|\mathbf{p}_b||\mathbf{q}|\cos\theta_b\cos\theta_1 - 2|\mathbf{p}_b||\mathbf{q}|\cos\theta_b + |\mathbf{p}_1||\mathbf{q}|\cos\theta_1. \end{aligned} \quad (\text{A10})$$

There are two additional constraints on the eight integration variables in Eq. (A7):

- a. For any configuration of the eight variables, Eq. (A9) must have at least one root.
- b. $E_a + E_b \geq E_1 + q_0 + m_2$.

APPENDIX B: GAUGE INVARIANCE OF PHOTON PRODUCTION AMPLITUDES

In this appendix, we demonstrate gauge invariance for the process $\pi^+\pi^- \rightarrow \pi^+\pi^-\gamma$. In this case the charges are, $Q_a = Q_1 = 1$, $Q_b = Q_2 = -1$, and there is no u -channel contribution. To verify $\mathcal{M}^\mu \cdot q_\mu = 0$ for the t -channel amplitude, we have

$$\begin{aligned} \mathcal{M}_t^\mu \cdot q_\mu &= e(J_a^\mu \mathcal{M}_t(p_a - q, p_b, p_1, p_2) + J_b^\mu \mathcal{M}_t(p_a, p_b - q, p_1, p_2) \\ &\quad + J_1^\mu \mathcal{M}_t(p_a, p_b, p_1 + q, p_2) + J_2^\mu \mathcal{M}_t(p_a, p_b, p_1, p_2 + q)) \cdot q_\mu \\ &= e(-\mathcal{M}_t(p_a - q, p_b, p_1, p_2) + \mathcal{M}_t(p_a, p_b - p_a, p_1, p_2) + \mathcal{M}_t(p_a, p_b, p_1 + q, p_2) - \mathcal{M}_t(p_a, p_b, p_1, p_2 + q)) \\ &= 4eg_\sigma^2 \pi \pi \left\{ F^2[(p_b - p_2)^2] \left[\frac{(p_a \cdot p_1 - q \cdot p_1)p_b \cdot p_2}{(p_b - p_2)^2 - m_\sigma^2 + im_\sigma \Gamma_\sigma} - \frac{(p_a \cdot p_1 + p_a \cdot q)p_b \cdot p_2}{(p_b - p_2)^2 - m_\sigma^2 + im_\sigma \Gamma_\sigma} \right] \right. \\ &\quad \left. + F[(p_a - p_1)^2] \left[-\frac{p_a \cdot p_1(p_b \cdot p_2 - q \cdot p_2)}{(p_a - p_1)^2 - m_\sigma^2 + im_\sigma \Gamma_\sigma} + \frac{p_a \cdot p_1(p_b \cdot p_2 + p_b \cdot q)}{(p_a - p_1)^2 - m_\sigma^2 + im_\sigma \Gamma_\sigma} \right] \right\} \\ &= 4eg_\sigma^2 \pi \pi \left[F^2[(p_b - p_2)^2] \frac{-(q \cdot p_1 + q \cdot p_a)p_b \cdot p_2}{(p_b - p_2)^2 - m_\sigma^2 + im_\sigma \Gamma_\sigma} + F^2[(p_a - p_1)^2] \frac{p_a \cdot p_1(q \cdot p_2 + q \cdot p_b)}{(p_a - p_1)^2 - m_\sigma^2 + im_\sigma \Gamma_\sigma} \right], \end{aligned} \quad (\text{B1})$$

so that the pertinent contact term is deduced as

$$\mathcal{M}_t^{(c)\mu} \cdot q_\mu = F^2[(p_b - p_2)^2] \frac{4eg_{\sigma\pi\pi}^2(p_a \cdot q + p_1 \cdot q)p_b \cdot p_2}{(p_b - p_2)^2 - m_\sigma^2 + im_\sigma\Gamma_\sigma} - F^2[(p_a - p_1)^2] \frac{4eg_{\sigma\pi\pi}^2 p_a \cdot p_1(p_b \cdot q + p_2 \cdot q)}{(p_a - p_1)^2 - m_\sigma^2 + im_\sigma\Gamma_\sigma}, \quad (\text{B2})$$

resulting in $\mathcal{M}_t^\mu \cdot q_\mu + \mathcal{M}_t^{(c)\mu} \cdot q_\mu = 0$. Similarly, for the s -channel, we have

$$\begin{aligned} \mathcal{M}_s^\mu \cdot q_\mu &= e(J_a^\mu \mathcal{M}_s(p_a - q, p_b, p_1, p_2) + J_b^\mu \mathcal{M}_s(p_a, p_b - q, p_1, p_2) \\ &\quad + J_1^\mu \mathcal{M}_s(p_a, p_b, p_1 + q, p_2) + J_2^\mu \mathcal{M}_s(p_a, p_b, p_1, p_2 + q)) \cdot q_\mu \\ &= e(-\mathcal{M}_s(p_a - q, p_b, p_1, p_2) + \mathcal{M}_s(p_a, p_b - p_a, p_1, p_2) + \mathcal{M}_s(p_a, p_b, p_1 + q, p_2) - \mathcal{M}_s(p_a, p_b, p_1, p_2 + q)) \\ &= 4eg_{\sigma\pi\pi}^2 \left[\frac{(p_a \cdot p_b - q \cdot p_b)p_1 \cdot p_2}{(p_1 + p_2)^2 - m_\sigma^2 + im_\sigma\Gamma_\sigma} - \frac{(p_a \cdot p_b - p_a \cdot q)p_1 \cdot p_2}{(p_1 + p_2)^2 - m_\sigma^2 + im_\sigma\Gamma_\sigma} \right. \\ &\quad \left. - \frac{p_a \cdot p_b(p_1 \cdot p_2 + q \cdot p_2)}{(p_a + p_b)^2 - m_\sigma^2 + im_\sigma\Gamma_\sigma} + \frac{p_a \cdot p_b(p_1 \cdot p_2 + p_1 \cdot q)}{(p_a + p_b)^2 - m_\sigma^2 + im_\sigma\Gamma_\sigma} \right] \\ &= 4eg_{\sigma\pi\pi}^2 \left[\frac{-(q \cdot p_b - q \cdot p_a)p_1 \cdot p_2}{(p_1 + p_2)^2 - m_\sigma^2 + im_\sigma\Gamma_\sigma} + \frac{p_a \cdot p_b(q \cdot p_1 - q \cdot p_2)}{(p_a + p_b)^2 - m_\sigma^2 + im_\sigma\Gamma_\sigma} \right] \end{aligned} \quad (\text{B3})$$

and the required contact term follows as

$$\mathcal{M}_s^{(c)\mu} \cdot q_\mu = \frac{4eg_{\sigma\pi\pi}^2(p_b \cdot q - p_a \cdot q)p_1 \cdot p_2}{(p_1 + p_2)^2 - m_\sigma^2 + im_\sigma\Gamma_\sigma} - \frac{4eg_{\sigma\pi\pi}^2 p_a \cdot p_b(p_1 \cdot q - p_2 \cdot q)}{(p_a + p_b)^2 - m_\sigma^2 + im_\sigma\Gamma_\sigma}. \quad (\text{B4})$$

Again, we arrive at $\mathcal{M}_s^\mu \cdot q_\mu + \mathcal{M}_s^{(c)\mu} \cdot q_\mu = 0$. It is straightforward to test the rho-meson exchange channels along similar lines.

APPENDIX C: RATE PARAMETERIZATIONS

The thermal production rate of photons from Bremsstrahlung off π - π and π - K scattering as employed in Sec. V can be conveniently parametrized as

$$\begin{aligned} q_0 \frac{dR_{\pi\pi}}{d^3q} &= \frac{-0.00026421 + \frac{0.0075394}{0.13007\sqrt{\pi/2}} \exp \left[\frac{-2(T-0.28351)^2}{0.13007^2} \right]}{0.01277} \\ &\quad \times \frac{-0.00018184 + \frac{0.00073983}{\pi[4(q_0-0.054587)^2+0.099656^2]}}{[1. + 104(0.18 - T)^{1.4}(q_0 - 0.1)]}, \\ q_0 \frac{dR_{\pi K}}{d^3q} &= \frac{-0.0000411907 + \frac{0.0013114}{0.12037\sqrt{\pi/2}} \exp \left[\frac{-2(T-0.27292)^2}{0.12037^2} \right]}{0.00227} \\ &\quad \times \frac{-0.000021454 + \frac{0.0001459}{\pi[4(q_0-0.043159)^2+0.085668^2]}}{[1. + 605(0.18 - T)^{1.7}(q_0 - 0.1)]} \end{aligned} \quad (\text{C1})$$

These expressions reproduce the exact rates within $\sim 3\%$ in the energy interval between 0.1 GeV and 0.5 GeV and in the temperature range 0.1-0.18 GeV. Pion and kaon chemical potentials are included as $\mu_\pi(T)$ and $\mu_K(T)$ according to the fireball evolution employed in this work for central $Pb(158 \text{ AGeV})$ - Pb collisions, cf. eq. (16). Temperature T and energy q_0 are in units of GeV, and the resulting rates are in units of $1/\text{GeV}^2\text{fm}^4$. For more general use, we also provide parameterizations which explicitly resolve the q_0 , T and μ_π dependencies:

$$q_0 \frac{dR_{\pi\pi}}{d^3q} = \frac{[1 + q_0/(0.011 + 0.56T - 0.565T^2)]^{-4}(0.92 + 0.17e^{\mu_\pi/0.0247})}{3(0.87 + 519e^{-T/0.026})(0.92 + 372e^{-T/0.026})}, \quad (\text{C2})$$

$$q_0 \frac{dR_{\pi K}}{d^3q} = \frac{[1 + q_0/(-0.024 + 0.773T)]^{-4}(0.8 + 0.223e^{\mu_K/0.05314})\sqrt{0.92 + 0.17e^{\mu_\pi/0.0247}}}{(14.87 + 3856e^{-T/0.032})\sqrt{0.92 + 372e^{-T/0.026}}(0.89 + 143e^{-T/0.026})} \quad (\text{C3})$$

These expressions reproduce the exact rates within $\sim 5\%$ in the energy interval between 0.1 GeV and 0.5 GeV and in the temperature range 0.1-0.18 GeV.

-
- [1] J. Alam, S. Sarkar, P. Roy, T. Hatsuda and B. Sinha, *Annals Phys.* **286**, 159 (2001).
 - [2] T. Peitzmann and M.H. Thoma, *Phys. Rep.* **364**, 175 (2002).
 - [3] F. Arleo *et al.*, arXiv:hep-ph/0311131.
 - [4] R. Rapp, *Mod. Phys. Lett.* **A19**, 1717 (2004).
 - [5] P. Stankus, *Ann. Rev. Nucl. Part. Sci.* **55**, 517 (2005).
 - [6] J. Kapusta, P. Lichard, and D. Seibert, *Phys. Rev. D* **44**, 2774(1991).
 - [7] C. Song, *Phys. Rev. C* **47**, 2861 (1993).
 - [8] V.V. Goloviznin and K. Redlich, *Phys. Lett.* **B319**, 520 (1993).
 - [9] P.K. Roy, D. Pal, S. Sarkar, D.K. Srivastava and B. Sinha, *Phys. Rev. C* **53**, 2364 (1996).
 - [10] J. Alam, P. Roy, and S. Sarkar, *Phys. Rev. C* **68**, 031901 (2003)
 - [11] S. Turbide, R. Rapp, and C. Gale, *Phys. Rev. C* **69**, 014903 (2004).
 - [12] K. L. Haglin, *J. Phys. G* **30**, L27 (2004).
 - [13] D.K. Srivastava, *Phys. Rev. C* **71**, 034905 (2005).
 - [14] WA98 Collaboration (M. M. Aggarwal *et al.*), *Phys. Rev. Lett.* **85**, 3595 (2000).
 - [15] WA98 Collaboration (M. M. Aggarwal *et al.*), *Phys. Rev. Lett.* **93**, 022301 (2004).
 - [16] S. Turbide, private communication (2004).
 - [17] R. Rapp, arXiv:nucl-th/0502020.
 - [18] R. Rückl, *Phys. Lett.* **B64**, 39 (1976).
 - [19] H.C. Eggers, R. Tabeti, C. Gale, and K. Haglin, *Phys. Rev. D* **53**, 4822 (1996).
 - [20] J. Cleymans, V. V. Goloviznin, and K. Redlich, *Phys. Rev. D* **47**, 173 (1993).
 - [21] J. Knoll and R. Lenk, *Nucl. Phys.* **A561**, 501(1993).
 - [22] K. Haglin, C. Gale, and V. Emel'yanov, *Phys. Rev. D* **47**, 973 (1993).
 - [23] C.H. Li and C.M. Ko, *Nucl. Phys.* **A712**, 110 (2002).
 - [24] J. F. Donoghue, C. Ramirez, and G. Valencia, *Phys. Rev. D* **39**, 1947 (1989).
 - [25] V. Srinivasan *et al.*, *Phys. Rev. D* **12**, 681 (1975); S. D. Protopoescu *et al.* *Phys. Rev. D* **7**, 1279 (1973).
 - [26] A. Firestone, G. Goldhaber, D. Lissauer, and G. H. Trilling, *Phys. Rev. D* **5**, 2188 (1972).
 - [27] R. Rapp, *Phys. Rev. C* **66**, 017901 (2002).
 - [28] R. Rapp and J. Wambach, *Eur. Phys. J.* **A6**, 415 (1999).
 - [29] L. Landau and I. Pomeranchuk, *Dokl. Akad. Nauk SSSR* **92**, 535 (1953); **92**, 735 (1953); A. B. Migdal, *Dokl. Akad. Nauk SSSR* **96**, 49 (1954); *Phys. Rev.* **103**, 1811 (1956).
 - [30] R. Rapp and J. Wambach, *Phys. Lett.* **B315**, 220 (1993).
 - [31] R. Rapp and J. Wambach, *Nucl. Phys.* **A573**, 626 (1994).
 - [32] G. Agakichiev *et al.* [CERES Collaboration], *Eur. Phys. J. C* **41**, 475 (2005).
 - [33] R. Arnaldi *et al.* [NA60 Collaboration], *Phys. Rev. Lett.* **96**, 162302 (2006).
 - [34] H. van Hees and R. Rapp, *Phys. Rev. Lett.* **97**, 102301 (2006).
 - [35] N. Grion *et al.* [CHAOS Collaboration], *Nucl. Phys.* **A763**, 80 (2005).
 - [36] A. Starostin *et al.* [Crystal Ball Collaboration], *Phys. Rev. Lett.* **85**, 5539 (2000).
 - [37] T. Hatsuda, T. Kunihiro, and H. Shimizu, *Phys. Rev. Lett.* **82**, 2840 (1999).
 - [38] D. Cabrera, E. Oset and M.J. Vicente Vacas, *Phys. Rev. C* **72**, 025207 (2005).
 - [39] D. Röder, arXiv:hep-ph/0509232.
 - [40] M.A. Halasz, J.V. Steele, G.Q. Li and G.E. Brown, *Phys. Rev. C* **58**, 365 (1998).
 - [41] C.s. Song and G. I. Fai, *Phys. Rev. C* **58**, 1689 (1998).
 - [42] J.e. Alam, P. Roy, S. Sarkar and B. Sinha, *Phys. Rev. C* **67**, 054901 (2003).
 - [43] P. Arnold, G.D. Moore and L.G. Yaffe, *JHEP* 0112 (2001) 009.
 - [44] R. Rapp, M. Urban, M. Buballa and J. Wambach, *Phys. Lett.* **B417**, 1 (1998).
 - [45] J. Bjorken and L. McLerran, *Phys. Rev. D* **31**, 63 (1985).
 - [46] C.M. Ko and C.Y. Wong, *Phys. Rev. C* **33**, 153 (1986).
 - [47] NA49 Collaboration (J. Bächler *et al.*), *Nucl. Phys.* **A661**, 45c (1999).